JOURNAL OF GUIDANCE, CONTROL, AND DYNAMICS
Vol. 19, No. 3, May–June 1996

Near-Optimal Highly Robust Guidance for Aeroassisted Orbital Transfer

A. Miele* and T. Wang†
Rice University, Houston, Texas 77251-1892

One of the difficulties in aeroassisted orbital transfer vehicle design is the complexity of the guidance scheme. In present aeroassisted orbital transfer guidance schemes, the reference value of the bank angle or the climb rate is determined via a predictor–corrector algorithm so that the desired apogee can be reached after the vehicle exits the atmosphere. These guidance schemes are quite sensitive to parameter dispersion effects due to atmospheric density errors, system errors, navigation errors, and aerodynamic coefficient errors. An innovative guidance scheme, called safety zone guidance, is developed. In this highly robust guidance, the control is not determined by aiming only at the desired apogee; instead, for each altitude–velocity pair, a special value of the path inclination is determined by maximizing the control margin while aiming at the desired apogee during the atmospheric pass. This results in a robust and accurate guidance scheme as shown by extensive numerical tests.

I. Introduction

IN space flight, there exist two kinds of orbital maneuvers: 1) transfer from a lower orbit to a higher orbit, requiring an increase in total energy and 2) transfer from a higher orbit to a lower orbit, requiring a decrease in total energy. Concerning transfer 2, propellant savings are possible if the all-propulsive mode is replaced by the synergetic mode, involving the combination of propulsive maneuvers in space with aerodynamic maneuvers in the atmosphere, hence the name aeroassisted orbital transfer (AOT).[1,2] AOT maneuvers can be used in Mars exploration/return vehicles, lunar return vehicles, and also near-Earth vehicles that must be transferred from a higher orbit to a lower orbit.

For an AOT vehicle, the benefits of propellant saving and payload increase must be weighted against the high-heating rates occurring during the atmospheric pass and the complexity of the guidance scheme.[3] To answer this challenge, considerable effort has been devoted during the last decade to the study of optimal trajectories and the development of guidance schemes.[4–7]

The objective of the atmospheric pass guidance is to deplete velocity so that, after exiting the atmosphere, the vehicle can ascend to the specified apogee in the specified orbital plane; of course, the peak heating rate during the atmospheric pass must be contained within acceptable levels. Because the angle of attack is held constant at the trim position [$\alpha = 17$ deg for the aeroassisted flight experiment (AFE) vehicle], the only control is the bank angle; thus, the modulus of the bank angle is used to control the longitudinal motion, whereas the sign of the bank angle is used to control the lateral motion.

Based on nominal trajectory analyses,[8] the AOT guidance includes two phases: entry phase and exit phase. The objective of the entry phase is to control the bank angle so as to contain the peak heating rate during the atmospheric pass. The objective of the exit phase is to control the bank angle so that the vehicle, after exiting the atmosphere in the specified orbital plane, can ascend to the specified apogee. In this paper, which continues the work initiated in Ref. 9, the focus is on developing the exit phase guidance for an AOT vehicle.[10] For the complete guidance, involving both the entry phase and the exit phase, see Ref. 11.

In developing the exit phase guidance, a major problem is to ensure that the specified apogee radius can be reached after the atmospheric pass, even in the presence of severe parameter dispersion effects, such as atmospheric density errors, system errors, navigation errors, and aerodynamic coefficient errors. An added difficulty is that, for an AFE type spacecraft, the longitudinal motion is intrinsically unstable and the lateral motion is nearly neutral. A further difficulty is caused by the nearly exponential decrease of the atmospheric density with the altitude.[12–14]

To overcome the cited difficulties, an innovative guidance scheme is developed, based on optimization theory and control margin theory.[8] The intent of this scheme, called safety zone guidance (SZG), is to guide the vehicle toward a special value of the path inclination for each given altitude–velocity pair. This special path inclination has the following property: it allows the vehicle to aim at the specified apogee with maximum control margin during the atmospheric pass.

As the subsequent analysis shows, the SZG is very robust to parameter dispersion effects and it allows the AOT vehicle to approach the specified apogee radius with high accuracy after completing the atmospheric pass. Indeed, the SZG is considerably more robust than alternative guidance schemes, such as the constant bank angle guidance (BAG), constant climb rate guidance (CRG), and constant path inclination guidance (PIG).

II. System Description

The motion of the AOT spacecraft takes place partly in space and partly in the atmosphere. For the purposes of this paper, the trajectory begins at geosynchronous Earth orbit (GEO) ($h = 35{,}786$ km) and ends at low Earth orbit (LEO) ($h = 330$ km). It includes a preatmospheric branch, an atmospheric branch, and a postatmospheric branch. We assume that GEO and LEO are coplanar circular orbits with orbital plane coincident with that of the Space Shuttle.

The key points of the maneuver are these: point 00, exit from GEO; point 0, atmospheric entry; point 1, atmospheric exit; point 11, entry into LEO. Point 00 is the apogee of the preatmospheric transfer orbit $00 \rightarrow 0$; point 11 is the apogee of the postatmospheric transfer orbit $1 \rightarrow 11$. Propulsive impulses are applied at two points: at point 00 to deorbit from GEO; at point 11 to circularize the motion into LEO; see Fig. 1.

For the atmospheric portion ($h \leq h_a$) of the trajectory of the AOT spacecraft, we employ an Earth-fixed system; for the space portion of the trajectory ($h > h_a$), we employ an inertial system; here, $h_a \cong 122$ km denotes the thickness of the atmosphere. For $h \leq h_a$, we compute the air density using the U.S. Standard Atmosphere, 1976[15]; for $h > h_a$, we assume that the air density is zero. For both the atmospheric portion and the space portion of the trajectory, we neglect the effects due to the oblateness of the Earth; we assume that the gravitational field is central and obeys the inverse square law.

With reference to the atmospheric portion of the trajectory of the AOT vehicle, the following additional hypotheses are employed:

Received Nov. 3, 1994; revision received Oct. 25, 1995; accepted for publication Oct. 28, 1995.

*A. J. Foyt Professor Emeritus of Engineering, Aerospace Sciences, and Mathematical Sciences, Aero-Astronautics Group.

†Senior Research Scientist, Aero-Astronautics Group.

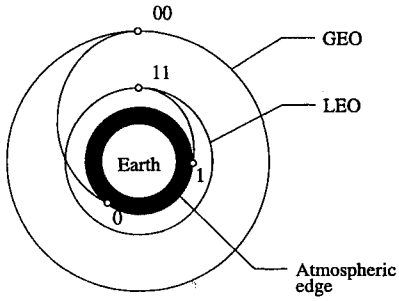

Fig. 1 Aeroassisted orbital transfer, GEO to LEO.

1) The atmospheric pass is made with the engine shut off; hence, the AOT spacecraft behaves as a particle of constant mass. 2) Under extreme hypersonic conditions, the dependence of the aerodynamic coefficients on the Mach number and the Reynolds number is disregarded. 3) The sideslip angle is zero; hence, the side force component of the aerodynamic force is zero. 4) The angle of attack is constant. 5) The AOT spacecraft is controlled via the angle of bank. (An example of spacecraft flying at constant angle of attack and variable angle of bank is the AFE spacecraft; see Ref. 14.)

A. Differential System

With the preceding assumptions and upon using an Earth-fixed system, the equations of motion[16] include the kinematical equations for the longitude θ, latitude ϕ, and radius r,

$$\dot{\theta} = \frac{V \cos\gamma \cos\chi}{r \cos\phi} \tag{1a}$$

$$\dot{\phi} = -\frac{V \cos\gamma \sin\chi}{r} \tag{1b}$$

$$\dot{r} = V \sin\gamma \tag{1c}$$

and the dynamical equations for the velocity V, path inclination γ, and heading angle χ,

$$\dot{V} = (-D/m) - g\sin\gamma + \omega^2 r(\sin\gamma\cos^2\phi + \cos\gamma\sin\chi\cos\phi\sin\phi) \tag{2a}$$

$$\dot{\gamma} = (L/mV)\cos\mu + [(V/r) - (g/V)]\cos\gamma + 2\omega\cos\chi\cos\phi + (\omega^2 r/V)(\cos\gamma\cos^2\phi - \sin\gamma\sin\chi\cos\phi\sin\phi) \tag{2b}$$

$$\dot{\chi} = \frac{L}{mV}\frac{\sin\mu}{\cos\gamma} + \frac{V}{r}\cos\gamma\cos\chi\tan\phi + 2\omega(\sin\phi + \tan\gamma\sin\chi\cos\phi) + \frac{\omega^2 r}{V}\frac{\cos\chi\cos\phi\sin\phi}{\cos\gamma} \tag{2c}$$

In the dynamical equations, D is the drag, L the lift, m the spacecraft mass, μ the angle of bank, and ω the angular velocity of the Earth; terms linear in ω are due to the Coriolis acceleration; terms quadratic in ω are due to the transport acceleration. Also in the dynamical equations, the local acceleration of gravity is given by

$$g = \mu_e/r^2 \tag{3}$$

where μ_e denotes the Earth gravitational constant. In addition, the aerodynamic forces are given by

$$D = \tfrac{1}{2}C_D(\alpha)\rho(h)SV^2 \tag{4a}$$

$$L = \tfrac{1}{2}C_L(\alpha)\rho(h)SV^2 \tag{4b}$$

where C_D is the drag coefficient, C_L the lift coefficient, S a reference surface area, and ρ the air density. The aerodynamic coefficients depend on the angle of attack α and the density depends on the altitude h, with

$$h = r - r_e \tag{4c}$$

where r_e is the Earth radius. Although the bank angle is unconstrained, its time rate is subject to the inequality

$$-A \le \dot{\mu} \le +A \tag{5}$$

where A is a prescribed constant.

For given initial conditions and controls $\alpha = \text{const}$ and $\mu = \mu(t)$, Eqs. (1) and (2) can be integrated forward in time over the time interval $0 \le t \le \tau$. Here, the initial time $t = 0$ corresponds to atmospheric entry, and the final time $t = \tau$ corresponds to atmospheric exit.

B. Entry Conditions

For the AOT vehicle, the examples considered in this paper assume that the entry conditions are given, that is, they have the form

$$\tilde{\theta}_0 = \text{given} \tag{6a}$$

$$\phi_0 = \text{given} \tag{6b}$$

$$r_0 = r_a \tag{6c}$$

$$\tilde{V}_0 = \text{given} \tag{6d}$$

$$\tilde{\gamma}_0 = \text{given} \tag{6e}$$

$$\tilde{\chi}_0 = \text{given} \tag{6f}$$

where the tilde superscript refers to quantities computed in an inertial system. Clearly, all of the state variables are given including $\tilde{V}_0$ and $\tilde{\gamma}_0$, which must be prescribed consistently with the relation

$$2\left(r_{00}^2 - r_{00}r_a\right)V_*^2 + \left(r_a^2\cos^2\tilde{\gamma}_0 - r_{00}^2\right)\tilde{V}_0^2 = 0 \tag{7}$$

This relation arises from energy conservation and angular momentum conservation applied to the preatmospheric transfer orbit $00 \rightarrow 0$ connecting GEO with atmospheric entry. Here, the symbol $V_* = \sqrt{(\mu_e/r_a)}$ denotes a reference velocity, that is, the circular velocity at $r = r_a$.

C. Exit Conditions

For the AOT vehicle, the desired exit conditions are given by

$$r_1 = r_a \tag{8a}$$

$$2\left(r_{11}^2 - r_{11}r_a\right)V_*^2 + \left(r_a^2\cos^2\tilde{\gamma}_1 - r_{11}^2\right)\tilde{V}_1^2 = 0 \tag{8b}$$

$$\tilde{i}_1 = \tilde{i}_0 \tag{8c}$$

$$\tilde{\Omega}_1 = \tilde{\Omega}_0 \tag{8d}$$

Clearly, the state variable r_1 is given; the state variables $\tilde{V}_1$ and $\tilde{\gamma}_1$ must be chosen consistently with Eq. (8b); and the state variables $\tilde{\theta}_1$, ϕ_1, and $\tilde{\chi}_1$ must be chosen consistently with Eqs. (8c) and (8d), where i denotes the orbital inclination and Ω the longitude of the ascending node. Equation (8b) arises from energy conservation and angular momentum conservation applied to the postatmospheric transfer orbit $1 \rightarrow 11$ connecting atmospheric exit with LEO. Equations (8c) and (8d) express the requirement that the exit orbital plane must be identical with the entry orbital plane.

D. Remark

For brevity of notation, the differential system (1) and (2) has been written in Earth-fixed coordinates, whereas the boundary conditions (6) and (8) have been written in inertial coordinates. General transformation relations allow one to pass from Earth-fixed quantities to inertial quantities and vice versa. Once the state variables are known in the inertial system, one can compute certain derived quantities, such as the orbital inclination $\tilde{i}$, longitude of the ascending node $\tilde{\Omega}$, wedge angle $\tilde{\eta}$, out-of-plane position angle $\tilde{\delta}$, and out-of-plane velocity angle $\tilde{\varepsilon}$. For details, see Refs. 9–11.

III. Guidance Concepts

The objective of the atmospheric pass guidance is to deplete velocity so that, after exiting the atmosphere, the vehicle can ascend to the specified apogee in the specified orbital plane; of course, the peak heating rate during the atmospheric pass must be contained within acceptable levels. Furthermore, the AOT vehicle must be able to safely execute the atmospheric pass even in the presence of severe environmental conditions, such as atmospheric density errors, system errors, navigation errors, and aerodynamic coefficient errors.

To achieve the listed goals, based on optimal trajectory analysis and control margin theory,[8] we decompose the atmospheric pass guidance into entry phase guidance and exit phase guidance. The objective of the entry phase guidance is to contain the peak heating rate within acceptable levels. The objective of the exit phase guidance is to steer the vehicle to the specified apogee in the specified orbital plane. The switch time t_s from entry phase to exit phase is to be determined as a compromise between the peak heating rate of the entry phase and the control margin of the exit phase.

In this paper, assuming that the switch time t_s has already been determined,[11] we focus our attention on exit phase guidance. The latter can be further decomposed into longitudinal guidance and lateral guidance. The objective of the longitudinal guidance is to achieve the specified apogee after exiting the atmosphere; the objective of the lateral guidance is to achieve the specified orbital plane at atmospheric exit.

Because the angle of attack is held constant at the trim position during the atmospheric pass ($\alpha = 17$ deg for the AFE spacecraft), the only control is the angle of bank μ. Thus, the modulus of the bank angle is used to control the longitudinal motion, whereas the sign of the bank angle is used to control the lateral motion.

We note that, for a typical AOT spacecraft, the longitudinal motion is highly unstable, whereas the lateral motion is nearly neutral.[9] Therefore, assuming that the control is fixed for the entry phase ($t \leq t_s$), we consider and compare various guidance strategies for the exit phase ($t \geq t_s$). Concerning the lateral motion, we assume that the control is determined via the out-of-plane velocity angle $\tilde{\varepsilon}$. Whenever $\tilde{\varepsilon}$ violates some prescribed altitude-dependent bounds,

$$-B(h) \leq \tilde{\varepsilon} \leq +B(h) \tag{9}$$

the bank angle changes sign.

With this understood, the generation of the bank angle value is done in three steps: 1) the modulus of the bank angle μ_p is obtained via the longitudinal motion control; 2) the command bank angle μ_c is obtained from μ_p after the sign of the bank angle has been determined via the lateral motion control; and 3) the real bank angle μ is obtained from μ_c in light of the bank angle time-rate constraint (5); see Fig. 2 and Refs. 10 and 11.

IV. Predictor–Corrector Algorithm

In this section, we present the predictor-corrector algorithm governing the exit phase guidance in four versions: SZG; constant BAG; constant CRG; and constant PIG. With SZG, one aims at the specified apogee while maintaining maximum control margin during the atmospheric pass. With BAG, CRG, and PIG, one aims at the specified apogee without consideration of control margin.

A. Differential System

Because use of the complete equations of motion (1) and (2) is expensive in terms of CPU time, we employ decomposition techniques decoupling the longitudinal motion from the lateral motion.[17] The decoupling is possible if the following approximations are introduced in Eqs. (1) and (2):

$$i \cong i_0 \tag{10a}$$

$$\omega^2 \cong 0 \tag{10b}$$

Approximation (10a) means that the instantaneous orbital plane is nearly identical with the entry orbital plane and implies that

$$\cos i_0 = \cos\phi \cos\chi \tag{11}$$

Approximation (10b) means that terms quadratic in ω (transport acceleration terms) are negligible with respect to terms linear in ω (Coriolis acceleration terms) and terms not containing ω.

With this understanding, the longitudinal motion is described by the following equations for the radius r, velocity V, and path inclination γ:

$$\dot{r} = V \sin\gamma \tag{12a}$$

$$\dot{V} = (-D/m) - g \sin\gamma \tag{12b}$$

$$\dot{\gamma} = (L/mV)\cos\mu + [(V/r) - (g/V)]\cos\gamma + 2\omega\cos i_0 \tag{12c}$$

in which the acceleration of gravity g, drag D, lift L, and altitude h are described by Eqs. (3) and (4) of Sec. II. For given initial conditions and controls $\alpha = \text{const}$ and $\mu = \mu(t)$ or $\mu = \mu(r, V, \gamma)$, Eqs. (12) can be integrated forward in time over the time interval $t_i \leq t \leq \tau$. Here, the initial time $t = t_i$ corresponds to the present position of the spacecraft, and the final time $t = \tau$ corresponds to atmospheric exit.

B. Control Law

For the guidance schemes under consideration, we investigate the following control laws.

SZG:

$$\cos\mu = 0 \tag{13a}$$

BAG:

$$\cos\mu = C \tag{13b}$$

CRG:

$$\cos\mu = (m/L)\big[(D/m)\tan\gamma + (g/\cos\gamma) - (V^2/r)\cos\gamma - 2\omega V\cos i_0\big] \tag{13c}$$

PIG:

$$\cos\mu = (m/L)\big[g\cos\gamma - (V^2/r)\cos\gamma - 2\omega V\cos i_0\big] \tag{13d}$$

These control laws, respectively, imply the following.

SZG:

$$\mu = \pi/2 \tag{14a}$$

BAG:

$$\mu = \text{const} \tag{14b}$$

CRG:

$$\dot{h} = \text{const} \tag{14c}$$

PIG:

$$\gamma = \text{const} \tag{14d}$$

hence maximum control margin,[8] constant bank angle, constant climb rate, and constant path inclination. Of course, each of the control laws (13) is subject to the inequality

$$-1 \leq \cos\mu \leq +1 \tag{15}$$

C. Initial Conditions

For the longitudinal motion system (12), the initial conditions (time $t = t_i$) are as follows.

SZG:

$$r_i = \text{given}, \qquad V_i = \text{given}, \qquad \gamma_i = \text{free} \tag{16a}$$

BAG:

$$r_i = \text{given}, \qquad V_i = \text{given}, \qquad \gamma_i = \text{given} \tag{16b}$$

CRG:

$$r_i = \text{given}, \qquad V_i = \text{given}, \qquad \gamma_i = \text{free} \tag{16c}$$

PIG:

$$r_i = \text{given}, \qquad V_i = \text{given}, \qquad \gamma_i = \text{free} \tag{16d}$$

Therefore, all of the state variables are given in the BAG; on the other hand, γ_i is free in the remaining guidance schemes.

D. Final Conditions

For the longitudinal motion system (12), the final conditions (time $t = \tau$) are as follows:

$$r_1 - r_a = 0 \tag{17a}$$

$$2\left(r_{11}^2 - r_{11}r_a\right)V_*^2 + 2\left(r_a^2 - r_{11}^2\right)\omega r_a V_1 \cos\gamma_1 \cos i_0 + \left(r_a^2 \cos^2\gamma_1 - r_{11}^2\right)V_1^2 = 0 \tag{17b}$$

Equation (17a) determines the final time τ of the atmospheric pass. Equation (17b) is a restatement of Eq. (8b) in light of the dynamic transformation equations[9–11] and the approximations (10).

E. Two-Point Boundary-Value Problem

For the guidance schemes under consideration, Eqs. (12–17) represent a nonlinear, two-point boundary-value problem (TPBVP) that can be solved with a one-dimensional search, on recognizing that the TPBVP is dominated by the following driving quantities: for the constant BAG, the value of the constant C in Eq. (13b); for the remaining guidance systems, the value of the initial path inclination γ_i in Eqs. (16a), (16c), or (16d). Once the driving quantity is prescribed, Eqs. (12) can be integrated forward in time subject to the appropriate control law (13) to yield the functions $r(t)$, $V(t)$, and $\gamma(t)$ over the time interval $t_i \leq t \leq \tau$, with τ determined by Eq. (17a). Then, the driving quantity of each guidance scheme must be determined so that Eq. (17b) is also satisfied. This requires a trial-and-error procedure, which can be speeded up via a process of linearization and/or bisection. Details are omitted for brevity.

F. Feedback Control

In the predictor–corrector algorithm, the TPBVP is solved every Δt seconds. Therefore, a feedback control law is needed for the time interval between successive solutions of the TPBVP, $t_i \leq t \leq t_i + \Delta t$.

In the SZG, let the functions $r(t)$, $V(t)$, and $\gamma(t)$ obtained from the solution of the TPBVP be regarded as parametric equations of the trajectory. For the time interval $t_i \leq t \leq t_i + \Delta t$, elimination of the parameter t from the functions $V(t)$ and $\gamma(t)$ yields the function $\gamma_*(V)$ that constitutes the safety zone during this time interval. Therefore, the following feedback control law is assumed [see Eqs. (13a) and (14a)]:

$$\cos\mu = \cos\mu_* + k\tan(\Delta\gamma) \tag{18a}$$

$$\Delta\gamma = \gamma - \gamma_*(V) \tag{18b}$$

$$\cos\mu_* = 0 \tag{18c}$$

where k is the gain coefficient and $\Delta\gamma$ is the deviation of the real path inclination γ from the computed safety zone path inclination $\gamma_*(V)$. Note that the function $\gamma_*(V)$, obtained by solving the TPBVP, must be updated every Δt seconds. Also note that, for small deviations, Eq. (18a) simplifies to

$$\cos\mu \cong \cos\mu_* + k\Delta\gamma \tag{18d}$$

In the constant BAG, Eqs. (18) are replaced by [see Eqs. (13b) and (14b)]

$$\cos\mu_p = \cos\mu_* \tag{19a}$$

$$\cos\mu_* = C \tag{19b}$$

Note that the constant C, obtained by solving the TPBVP, must be updated every Δt seconds.

In the constant CRG, Eqs. (18) are replaced by [see Eqs. (13c) and (14c)]

$$\cos\mu_p = \cos\mu_* + k(\rho_R/\rho)\Delta\dot{h} \tag{20a}$$

$$\Delta\dot{h} = \dot{h} - \dot{h}_{i*} \tag{20b}$$

$$\cos\mu_* = (m/L)\left[(D/m)\tan\gamma + (g/\cos\gamma) - (V^2/r)\cos\gamma - 2\omega V\cos i_0\right] \tag{20c}$$

where ρ is the density at altitude h, ρ_R a reference density at altitude $h_R = 60$ km, and $\Delta\dot{h}$ the deviation of the real climb rate $\dot{h}$ from the computed initial climb rate $\dot{h}_{i*}$. Note that the constant $\dot{h}_{i*}$ obtained by solving the TPBVP must be updated every Δt seconds.

In the constant PIG, Eqs. (18) are replaced by [see Eqs. (13d) and (14d)]

$$\cos\mu_p = \cos\mu_* + k(\rho_R/\rho)\Delta\gamma \tag{21a}$$

$$\Delta\gamma = \gamma - \gamma_{i*} \tag{21b}$$

$$\cos\mu_* = (m/L)\left[g\cos\gamma - (V^2/r)\cos\gamma - 2\omega V\cos i_0\right] \tag{21c}$$

with $\Delta\gamma$ the deviation of the real path inclination γ from the computed initial path inclination γ_{i*}. Note that the constant γ_{i*}, obtained by solving the TPBVP, must be updated every Δt seconds.

G. Remark

In the feedback control laws (18–21), the values of $\cos\mu_p$ and $\cos\mu_*$ are subject to inequality (15).

V. Dispersion Effects

In real AOT flights, there are dispersion effects arising from atmospheric density errors, system errors, navigation errors, and aerodynamic coefficient errors.

Let the subscript n denote a nominal condition; let the subscript e denote an estimated condition; and let the absence of a subscript denote a real condition. With this understanding, the following dispersion factors can be defined:

$$F_\rho = \frac{\rho(h)}{\rho_n(h)}, \qquad F_s = \frac{t_s}{t_{sn}}, \qquad F_\gamma = \frac{\tilde{\gamma}_0}{\tilde{\gamma}_{0n}} \tag{22a}$$

$$F_D = C_D/C_{Dn}, \qquad F_L = C_L/C_{Ln} \tag{22b}$$

and

$$F_{\rho e} = \frac{\rho_e(h)}{\rho_n(h)}, \qquad F_{se} = \frac{t_{se}}{t_{sn}}, \qquad F_{\gamma e} = \frac{\tilde{\gamma}_{0e}}{\tilde{\gamma}_{0n}} \tag{23a}$$

$$F_{De} = C_{De}/C_{Dn}, \qquad F_{Le} = C_{Le}/C_{Ln} \tag{23b}$$

The dispersion factors (22) are the ratios of real quantities to nominal quantities and are used in connection with the integration of the three-dimensional equations of motion (1) and (2) simulating the real environment. The dispersion factors (23) are the ratios of estimated quantities to nominal quantities and are used in connection with the integration of the two-dimensional equations of motion (12) employed in the predictor–corrector algorithm.

Clearly, the goodness of a guidance scheme is measured by the range of values of the dispersion factors (22) and (23) for which the AOT spacecraft can safely execute the atmospheric pass.

VI. Evaluation Criteria

In studying the effect of the dispersion factors (22) and (23) on the atmospheric pass, certain physical quantities must be considered: the peak heating rate, the minimum altitude, the control margin index, the apogee altitude, and the characteristic velocity. In this paper, we restrict our attention on the last two quantities. For extended information on the remaining physical quantities, see Refs. 10 and 11.

A. Apogee Altitude

Use of the energy and angular momentum conservation laws for the transfer orbit connecting the atmospheric exit point (radius r_a) and the apogee point (radius r_{22} generally different from r_{11}) yields the following relation:

$$r_{22} = \frac{r_a \tilde{V}_1^2 \cos^2 \tilde{\gamma}_1}{V_*^2 - \sqrt{\left(V_*^2 - \tilde{V}_1^2\right)^2 \cos^2 \tilde{\gamma}_1 + V_*^4 \sin^2 \tilde{\gamma}_1}} \tag{24a}$$

with the implication that

$$h_{22} = r_{22} - r_e \tag{24b}$$

Hence, the error in apogee altitude is

$$h_{22} - h_{11} = r_{22} - r_{11} \tag{24c}$$

where r_{11} is the desired LEO radius.

If the guidance is hypothetically perfect, the differences in Eq. (24c) vanish, which is the same as stating that Eq. (24a) is satisfied with r_{22} replaced by r_{11}.

B. Characteristic Velocity

Assuming that $r_{22} \geq r_{11}$, this includes two parts: the velocity impulse $\Delta \tilde{V}_{22}$ at apogee and the velocity impulse $\Delta \tilde{V}_{11}$ at perigee (LEO), that is,

$$\Delta \tilde{V} = \Delta \tilde{V}_{22} + \Delta \tilde{V}_{11} \tag{25a}$$

$$\Delta \tilde{V}_{22} = \sqrt{\frac{r_{11} r_a}{r_{22} r_{33}}} V_* - \frac{r_a}{r_{22}} \tilde{V}_1 \cos \tilde{\gamma}_1 \tag{25b}$$

$$\Delta \tilde{V}_{11} = -\sqrt{\frac{r_a}{r_{11}}} V_* + \sqrt{\frac{r_{22} r_a}{r_{11} r_{33}}} V_* \tag{25c}$$

where

$$r_{33} = \frac{r_{22} + r_{11}}{2} \tag{25d}$$

denotes the average radius between r_{22} and r_{11}.

If the guidance is hypothetically perfect, $r_{11} = r_{22} = r_{33}$; the right-hand side of Eq. (25c) vanishes; the characteristic velocity reduces to

$$\Delta \tilde{V} = \sqrt{(r_a/r_{11})} V_* - (r_a/r_{11}) \tilde{V}_1 \cos \tilde{\gamma}_1 \tag{26}$$

Note that Eqs. (25) and (26) do not include the GEO characteristic velocity $\Delta \tilde{V}_{00}$. This is because in the numerical experiments of Sec. VIII, the comparison of guidance schemes is done for fixed entry conditions; hence, for each given entry path inclination $\tilde{\gamma}_0$, $\Delta \tilde{V}_{00}$ must be regarded as a constant, independent of the particular guidance scheme being considered.

VII. Experimental Data

In the numerical experiments of Sec. VIII, the AOT vehicle is the AFE spacecraft (see Refs. 3 and 9–11).

A. Mission

The mission being simulated is the transfer from GEO (h_{00} = 35,786 km, corresponding to r_{00} = 42,164 km) to LEO (h_{11} = 330 km, corresponding to r_{11} = 6708 km). The AFE spacecraft, to be released and then recaptured by the Space Shuttle, enters and exits the atmosphere in the same orbital plane as that of the Space Shuttle, with orbital inclination $\tilde{i}$ = 28.45 deg and longitude of the ascending node $\tilde{\Omega} = -126.19$ deg. The simulated entry conditions correspond to a return from GEO.

B. Spacecraft

The mass of the AFE spacecraft is m = 1678 kg; the reference surface area is S = 14.31 m^2. For this configuration, the angle of attack is constant, α = 17.0 deg. At this angle of attack,

$$C_D = 1.355, \qquad C_L = -0.381 \tag{27a}$$

$$E = 0.281, \qquad C_M = 0.000 \tag{27b}$$

where E is the lift-to-drag ratio modulus and C_M the moment coefficient.

C. Physical Constants

The radius of the Earth is $r_e = 6378$ km; the radius of the outer edge of the atmosphere is $r_a = 6500$ km; the thickness of the atmosphere is $h_a = 122$ km; the Earth gravitational constant is $\mu_e = 0.3986E{+}06$ km^3/s^2; the reference velocity is $V_* = 7.831$ km/s; the angular velocity of the Earth is $\omega = 0.7292E{-}04$ rad/s.

The assumed atmospheric model is that of the U.S. Standard Atmosphere, 1976.[15]

D. Entry Conditions

In the inertial system, the given entry conditions are as follows: longitude $\tilde{\theta}_0 = -134.52$ deg; latitude $\phi_0 = -4.49$ deg; altitude $h_0 = 122$ km, corresponding to the radius $r_0 = 6500$ km; heading angle $\tilde{\chi}_0 = -28.13$ deg; orbital inclination $\tilde{i}_0 = 28.45$ deg; longitude of the ascending node $\tilde{\Omega}_0 = -126.19$ deg.

E. Exit Conditions

In the inertial system, the desired exit conditions are as follows: altitude $h_1 = 122$ km, corresponding to the radius $r_1 = 6500$ km; orbital inclination $\tilde{i}_0 = 28.45$ deg; longitude of the ascending node $\tilde{\Omega}_0 = -126.19$ deg.

F. Nominal Values

With reference to the dispersion factors (22) and (23) and the AFE spacecraft, the nominal values in Eqs. (22) and (23) are as follows:

$$\rho_n(h) = \text{density of the 1976 U.S. Standard Atmosphere} \tag{28a}$$

$$t_{sn} = 137.0\,\text{s}, \qquad \tilde{\gamma}_{0n} = -4.46\,\text{deg} \tag{28b}$$

$$C_{Dn} = 1.355, \qquad C_{Ln} = -0.381 \tag{28c}$$

G. Bank Angle

For all of the guidance schemes, the only control is the bank angle μ. The values of $\cos \mu$ entering the predictor–corrector algorithm are subject to inequality (15). The time rate of the bank angle $\dot{\mu}$ is subject to inequality (5), with

$$A = 15.0\,\text{deg/s} \tag{29}$$

H. Entry Phase

For all of the guidance schemes, the entry phase control $\mu(t)$ is fixed, specifically,

$$\mu = 190, \qquad 0 \leq t \leq t_1 \tag{30a}$$

$$\mu = 190 - 15t, \qquad t_1 \leq t \leq t_2 \tag{30b}$$

$$\mu = 0, \qquad t_2 \leq t \leq t_3 \tag{30c}$$

with μ in degrees, t in seconds, and

$$t_1 = 83.5, \qquad t_2 = 96.2, \qquad t_3 = 137.0 \tag{31}$$

Let t_s denote the switch time from entry phase to exit phase. Three cases must be considered:

1) Case where $0 \leq t_s \leq t_1$: the entry phase control reduces to Eq. (30a) with t_1 replaced by t_s.

2) Case where $t_1 \leq t_s \leq t_2$: the entry phase control reduces to Eq. (30a) → Eq. (30b), with t_2 replaced by t_s.

3) Case where $t_2 \leq t_s \leq t_3$: the entry phase control reduces to Eq. (30a) → Eq. (30b) → Eq. (30c), with t_3 replaced by t_s.

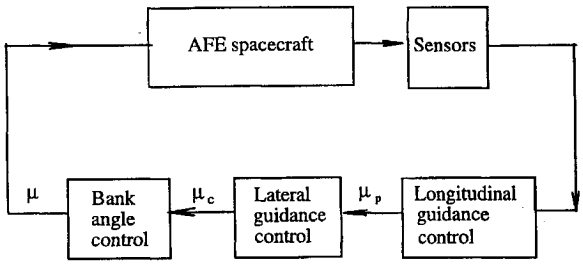

Fig. 2 Operational diagram, AFE spacecraft guidance and control system.

I. Exit Phase

For all of the guidance schemes, the exit phase control $\mu(t)$ is obtained in three steps (see Fig. 2).

1) The predicted bank angle modulus $\mu_p(t)$ is obtained via the longitudinal motion control, specifically via the predictor–corrector algorithm of Sec. IV.

2) The command bank angle $\mu_c(t)$ is obtained from $\mu_p(t)$ in light of inequality (9), where

$$B = 0.52, \qquad 60 \le h \le 75 \tag{32a}$$

$$B = 0.52 - 0.44(h - 75)/9, \qquad 75 \le h \le 84 \tag{32b}$$

$$B = 0.08 - 0.03(h - 84)/11, \qquad 84 \le h \le 95 \tag{32c}$$

$$B = 0.05, \qquad 95 \le h \le 122 \tag{32d}$$

with B in degrees and h in kilometers. Whenever the out-of-plane velocity angle $\tilde{\varepsilon}$ violates inequality (9), the command bank angle changes sign.

3) The real bank angle $\mu(t)$ is obtained from $\mu_c(t)$ in light of the bank angle time-rate constraint (5), with A given by Eq. (29).

VIII. Numerical Results

The objective of the numerical tests was to compare the behavior of the SZG, constant BAG, constant CRG, and constant PIG with respect to dispersion effects due to various causes: atmospheric density errors, switch time errors, entry path inclination errors, and aerodynamic coefficient errors.

A. Atmospheric Density Errors

The first group of tests was made assuming that

$$F_s = 1, \qquad F_\gamma = 1, \qquad F_D = 1, \qquad F_L = 1 \tag{33a}$$

$$F_{se} = 1, \qquad F_{\gamma e} = 1, \qquad F_{De} = 1, \qquad F_{Le} = 1 \tag{33b}$$

implying, in particular, that $\tilde{\gamma}_0 = -4.46$ deg, $t_s = 137$ s. Concerning the density, it was assumed that

$$F_\rho = 0.80 \tag{33c}$$

$$F_{\rho e} = 0.80, 0.85, 0.90, 0.95, 1.00 \tag{33d}$$

Clearly, the pair $(F_\rho, F_{\rho e}) = (0.8, 0.8)$ corresponds to perfect density estimation, whereas the pair $(F_\rho, F_{\rho e}) = (0.8, 1.0)$ corresponds to 25% error in the density estimation.

Figures 3 and 4 show the apogee altitude h_{22} and characteristic velocity $\Delta\tilde{V}$ vs the estimated density factor $F_{\rho e}$ for two guidance schemes: SZG and BAG. The results for CRG and PIG are not shown, since the behavior of these guidance schemes is the same as or worse than BAG. For SZG, the values of h_{22} and $\Delta\tilde{V}$ are roughly independent of $F_{\rho e}$; for BAG, they increase roughly linearly with $F_{\rho e}$.

For $F_{\rho e} = 0.8$, the values of h_{22} and $\Delta\tilde{V}$ are nearly the same for SZG and BAG. For $F_{\rho e} = 1$, however, the values of h_{22} and $\Delta\tilde{V}$ for BAG are 4–5 times higher than the corresponding values for SZG; thus, the superiority of SZG vis-a-vis BAG (hence, CRG and PIG) is clearly shown.

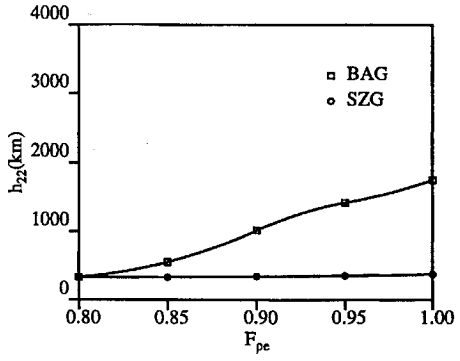

Fig. 3 Apogee altitude vs estimated density factor, $F_\rho = 0.8$.

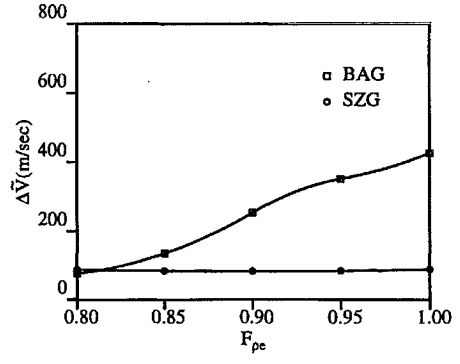

Fig. 4 Characteristic velocity vs estimated density factor, $F_\rho = 0.8$.

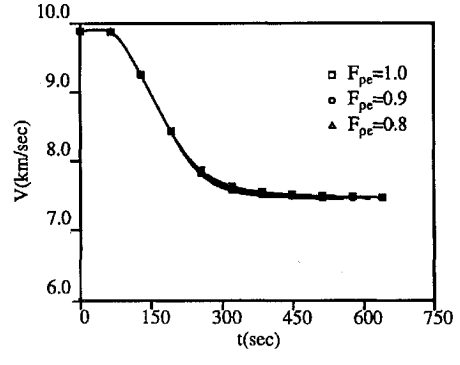

Fig. 5 SZG trajectory robustness, relative velocity vs time, $F_\rho = 0.8$.

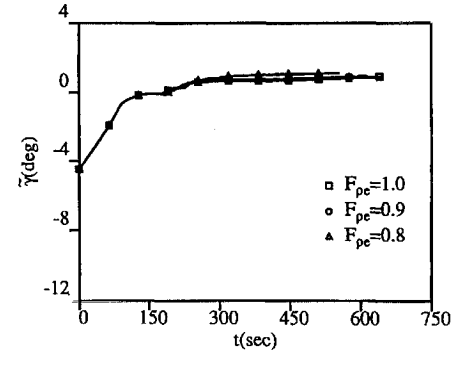

Fig. 6 SZG trajectory robustness, path inclination vs time, $F_\rho = 0.8$.

Figures 5 and 6 (SZG) and Figs. 7 and 8 (BAG) refer to trajectory robustness and show the time histories of the relative velocity $V(t)$ and inertial path inclination $\tilde{\gamma}(t)$ for three values of the estimated density factor $F_{\rho e}$. For SZG, the functions $V(t)$ and $\tilde{\gamma}(t)$ exhibit a mild dependence on $F_{\rho e}$; for BAG, they exhibit a strong dependence on $F_{\rho e}$. For BAG, the atmospheric exit takes place with higher values of the velocity and inertial path inclination than for SZG; this leads to considerable overshooting of the LEO ($h_{22} \gg h_{11}$) and, hence,

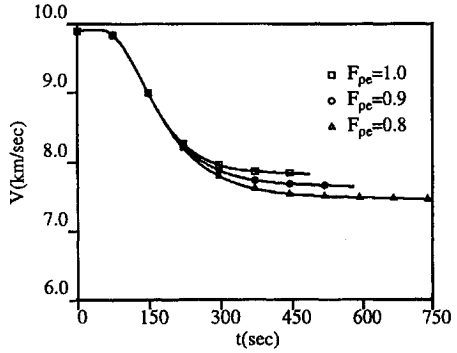

Fig. 7 BAG trajectory robustness, relative velocity vs time, $F_\rho = 0.8$.

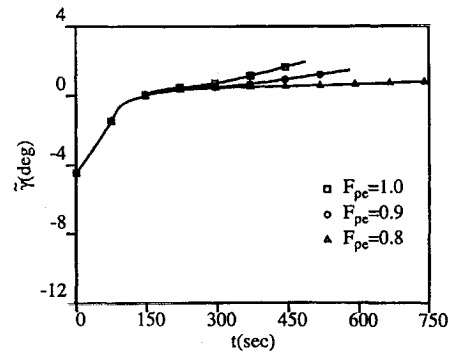

Fig. 8 BAG trajectory robustness, path inclination vs time, $F_\rho = 0.8$.

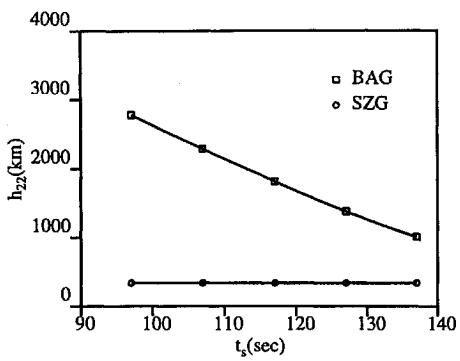

Fig. 9 Apogee altitude vs switch time.

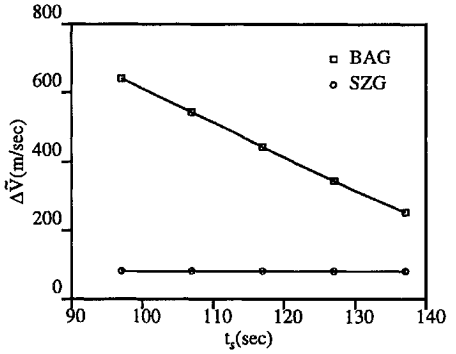

Fig. 10 Characteristic velocity vs switch time.

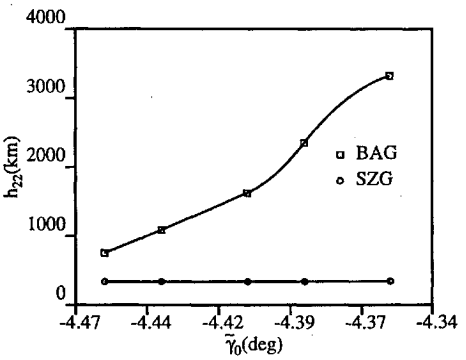

Fig. 11 Apogee altitude vs entry path inclination.

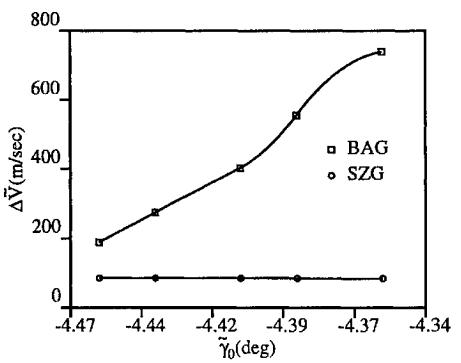

Fig. 12 Characteristic velocity vs entry path inclination.

considerable increase in the characteristic velocity $\Delta\tilde{V}$ required for circularization of the motion into LEO.

B. Switch Time Errors

The second group of tests was made assuming that

$$F_\rho = 0.8, \qquad F_\gamma = 1, \qquad F_D = 1, \qquad F_L = 1 \tag{34a}$$

$$F_{\rho e} = 0.9, \qquad F_{\gamma e} = 1, \qquad F_{De} = 1, \qquad F_{Le} = 1 \tag{34b}$$

implying, in particular, that $\tilde{\gamma}_0 = -4.46$ deg. Concerning the switch time, it was assumed that

$$F_s = F_{se} = 1.000, 0.927, 0.854, 0.781, 0.708 \tag{34c}$$

corresponding to

$$t_s = t_{se} = 137, 127, 117, 107, 97\,\text{s} \tag{34d}$$

Clearly, $F_s = 1$ corresponds to nominal switch, whereas $F_s = 0.708$ corresponds to early switch by nearly 29% timewise.

Figures 9 and 10 show the apogee altitude h_{22} and characteristic velocity $\Delta\tilde{V}$ vs the switch time t_s for two guidance schemes: SZG and BAG. The results for CRG and PIG are not shown, since they are the same as or worse than BAG. For SZG, the values of h_{22} and $\Delta\tilde{V}$ are roughly independent of t_s; for BAG, they change roughly linearly with t_s. In the range of switch times considered, the values of h_{22} and $\Delta\tilde{V}$ for BAG are 3–8 times larger than the corresponding values for SZG; thus, the superiority of SZG vis-a-vis BAG is clearly shown.

C. Entry Path Inclination Errors

The third group of tests was made assuming that

$$F_\rho = 0.8, \qquad F_s = 0.526, \qquad F_D = 1, \qquad F_L = 1 \tag{35a}$$

$$F_{\rho e} = 0.9, \qquad F_{se} = 0.526, \qquad F_{De} = 1, \qquad F_{Le} = 1 \tag{35b}$$

implying, in particular, that $t_s = 72$ s. Concerning the entry path inclination, it was assumed that

$$F_\gamma = F_{\gamma e} = 1.000, 0.996, 0.989, 0.984, 0.978 \tag{35c}$$

corresponding to

$$\tilde{\gamma}_0 = \tilde{\gamma}_{0e} = -4.46, -4.44, -4.41, -4.39, -4.36\,\text{deg} \tag{35d}$$

Clearly, $F_\gamma = 1$ corresponds to nominal entry, whereas $F_\gamma = 0.978$ corresponds to flatter entry by 0.1 deg.

Figures 11 and 12 show the apogee altitude h_{22} and characteristic velocity $\Delta\tilde{V}$ vs the entry path inclination $\tilde{\gamma}_0$ for two guidance

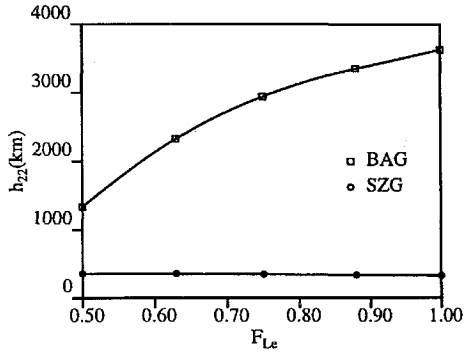

Fig. 13 Apogee altitude vs estimated lift factor, $F_L = 0.5$.

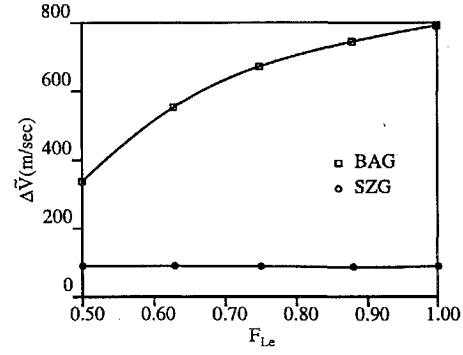

Fig. 14 Characteristic velocity vs estimated lift factor, $F_L = 0.5$.

schemes: SZG and BAG. The results for CRG and PIG are not shown, since they are the same as or worse than BAG. For SZG, the values of h_{22} and $\Delta\tilde{V}$ are roughly independent of $\tilde{\gamma}_0$; for BAG, they change roughly quadratically with $\tilde{\gamma}_0$. In the range of entry path inclinations considered, the values of h_{22} and $\Delta\tilde{V}$ for BAG are 2–10 times larger than the corresponding values for SZG; thus, the superiority of SZG vis-a-vis BAG is clearly shown.

D. Lift Coefficient Errors

The fourth group of tests was made assuming that

$$F_\rho = 0.9, \quad F_s = 0.398, \quad F_\gamma = 0.978, \quad F_D = 1 \tag{36a}$$

$$F_{\rho e} = 1.0, \quad F_{se} = 0.398, \quad F_{\gamma e} = 0.978, \quad F_{De} = 1 \tag{36b}$$

implying, in particular, that $t_s = 54.5$ s, $\tilde{\gamma}_0 = -4.36$ deg. Concerning the lift coefficient, it was assumed that

$$F_L = 0.50 \tag{36c}$$

$$F_{Le} = 0.50, 0.63, 0.75, 0.88, 1.00 \tag{36d}$$

Clearly, $F_{Le} = 0.5$ corresponds to perfect lift coefficient estimation and $F_{Le} = 1.00$ corresponds to 100% error in the lift coefficient estimation.

Figures 13 and 14 show the apogee altitude h_{22} and characteristic velocity $\Delta\tilde{V}$ vs the estimated lift coefficient factor F_{Le} for two guidance schemes: SZG and BAG. The results for CRG and PIG are not shown, since they are the same as or worse than BAG. For SZG, the values of h_{22} and $\Delta\tilde{V}$ are roughly independent of F_{Le}; for BAG, they change roughly quadratically with F_{Le}. In the range of estimated lift coefficient factors considered, the values of h_{22} and $\Delta\tilde{V}$ for BAG are 4–11 times larger than the corresponding values for SZG; thus, the superiority of SZG vis-a-vis BAG is clearly shown.

IX. Conclusions

In this paper, the atmospheric pass of an AOT spacecraft is considered and an SZG scheme is developed. The essence of the SZG scheme is that, for any instantaneous altitude–velocity pair, the spacecraft is guided to a special path inclination leading toward the desired LEO with maximum control margin.

Extensive numerical tests were made comparing SZG with constant BAG, constant CRG, and constant PIG. From these tests, the following conclusions can be made:

1) SZG enables the spacecraft to approach the specified LEO with high accuracy following the atmospheric pass.

2) SZG is extremely robust vis-a-vis dispersion effects due to atmospheric density errors, system errors, navigation errors, and aerodynamic coefficient errors.

3) SZG is considerably more robust than BAG, CRG, and PIG.

4) The explanation for these properties lies in the fact that SZG is constructed so as to maximize controllability while completing the atmospheric pass and aiming at the desired LEO; on the other hand, BAG, CRG, and PIG are constructed by aiming only at the desired LEO, while ignoring the controllability issue.

Acknowledgments

This research was supported by NASA Marshall Space Flight Center, Grant NAG-8-187, and by Texas Advanced Technology Program, Grant TATP-00360402O. This paper was presented by the first author at the 45th Congress of the International Astronautical Federation, Jerusalem, Israel, Oct. 9–14, 1994 (Paper IAF-94-A.2.011).

References

[1]Walberg, G. D., "A Survey of Aeroassisted Orbit Transfer," *Journal of Spacecraft and Rockets*, Vol. 22, No. 1, 1985, pp. 3–18.

[2]Braun, R. D., and Powell, R. W., "Aerodynamic Requirements of a Manned Mars Aerobraking Transfer Vehicle," *Journal of Spacecraft and Rockets*, Vol. 28, No. 4, 1991, pp. 361–367.

[3]Anon., "Aeroassisted Flight Experiment: Preliminary Design Document," NASA Marshall Space Flight Center, Huntsville, AL, 1986.

[4]Mease, K. D., and Vinh, N. X., "Minimum-Fuel Aeroassisted Coplanar Orbit Transfer Using Lift Modulation," *Journal of Guidance, Control, and Dynamics*, Vol. 8, No. 1, 1985, pp. 134–141.

[5]Miele, A., Basapur, V. K., and Mease, K. D., "Nearly-Grazing Optimal Trajectories for Aeroassisted Orbital Transfer," *Journal of the Astronautical Sciences*, Vol. 34, No. 1, 1986, pp. 3–18.

[6]Miele, A., Basapur, V. K., and Lee, W. Y., "Optimal Trajectories for Aeroassisted, Coplanar Orbital Transfer," *Journal of Optimization Theory and Applications*, Vol. 52, No. 1, 1987, pp. 1–24.

[7]Miele, A., Wang, T., Lee, W. Y., and Zhao, Z. G., "Optimal Trajectories for the Aeroassisted Flight Experiment," *Acta Astronautica*, Vol. 21, Nos. 11, 12, 1990, pp. 735–747.

[8]Miele, A., and Wang, T., "Nominal Trajectories for the Aeroassisted Flight Experiment," *Journal of the Astronautical Sciences*, Vol. 41, No. 2, 1993, pp. 139–163.

[9]Miele, A., and Wang, T., "AOT Guidance Analysis, Part 1: Nominal Trajectories," Aero-Astronautics Rept. 262, Rice Univ., Houston, TX, 1992 (revised 1993).

[10]Miele, A., and Wang, T., "AOT Guidance Analysis, Part 2: Safety Zone Guidance," Aero-Astronautics Rept. 266, Rice Univ., Houston, TX, 1993.

[11]Miele, A., and Wang, T., "AOT Guidance Analysis, Part 3: High Performance/Robustness Guidance," Aero-Astronautics Rept. 267, Rice Univ., Houston, TX, 1993.

[12]Miele, A., and Wang, T., "Gamma Guidance of Trajectories for Coplanar, Aeroassisted Orbital Transfer," *Journal of Guidance, Control, and Dynamics*, Vol. 15, No. 1, 1992, pp. 255–262.

[13]Dukeman, G. A., "A Generalized Reusable Guidance Algorithm for Optimal Aerobraking," NASA TM 103590, 1992.

[14]Gamble, J. D., Cerimele, C. J., Moore, T. E., and Higgins, J., "Atmospheric Guidance Concepts for an Aeroassist Flight Experiment," *Journal of the Astronautical Sciences*, Vol. 36, Nos. 1, 2, 1988, pp. 45–71.

[15]Anon., "US Standard Atmosphere, 1976," National Oceanic and Atmospheric Adminstration, NASA, and U.S. Air Force, U.S. Government Printing Office, Washington, DC, 1976.

[16]Miele, A., Zhao, Z. G., and Lee, W. Y., "Optimal Trajectories for the Aeroassisted Flight Experiment, Part 1: Equations of Motion in an Earth-Fixed System," Aero-Astronautics Rept. 238, Rice Univ., Houston, TX, 1989.

[17]Miele, A., Wang, T., and Deaton, A. W., "Decomposition Technique and Optimal Trajectories for the Aeroassisted Flight Experiment," *Journal of Optimization Theory and Applications*, Vol. 69, No. 2, 1991, pp. 201–234.